

Role of the intercalated ions on the high capacitance behavior of $Ti_3C_2T_x$ MXene nanohybrids

Bhargavi Koneru, Jhilmil Swapnalin, Ramyakrishna Pothu, Prasun Banerjee, Rajender Boddula, Ahmed Bahgat Radwan & Noora Al-Qahtani

To cite this article: Bhargavi Koneru, Jhilmil Swapnalin, Ramyakrishna Pothu, Prasun Banerjee, Rajender Boddula, Ahmed Bahgat Radwan & Noora Al-Qahtani (2023) Role of the intercalated ions on the high capacitance behavior of $Ti_3C_2T_x$ MXene nanohybrids, *Nanocomposites*, 9:1, 128-137, DOI: [10.1080/20550324.2023.2258622](https://doi.org/10.1080/20550324.2023.2258622)

To link to this article: <https://doi.org/10.1080/20550324.2023.2258622>



© 2023 The Author(s). Published by Informa UK Limited, trading as Taylor & Francis Group



Published online: 12 Sep 2023.



Submit your article to this journal [↗](#)



Article views: 722



View related articles [↗](#)



View Crossmark data [↗](#)



Citing articles: 2 View citing articles [↗](#)

Role of the intercalated ions on the high capacitance behavior of $Ti_3C_2T_x$ MXene nanohybrids

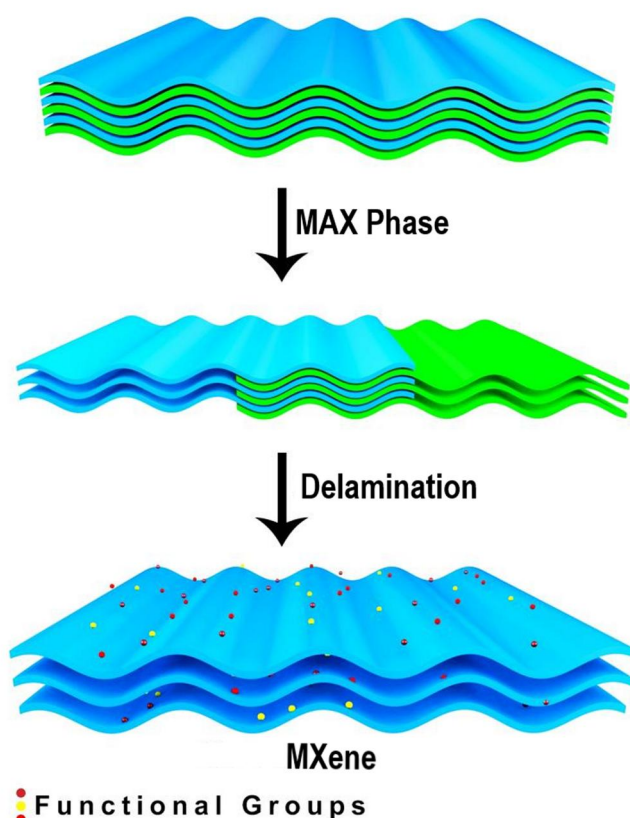
Bhargavi Koneru^a , Jhilmil Swapnalina^a , Ramyakrishna Pothu^b , Prasun Banerjee^a ,
Rajender Boddula^c , Ahmed Bahgat Radwan^c  and Noora Al-Qahtani^{c,d} 

^aGandhi Institute of Technology and Management (GITAM) University, Multiferroic and Magnetic Material Research Laboratory, Bengaluru, Karnataka, India; ^bSchool of Physics and Electronics, College of Chemistry and Chemical Engineering, Hunan University, Changsha, China; ^cCenter for Advanced Materials (CAM), Qatar University, Doha, Qatar; ^dCentral Laboratories Unit (CLU), Qatar University, Doha, Qatar

ABSTRACT

$Ti_3C_2T_x$ (MXene) is prone to surface oxidation because of the presence of oxygen surface terminals in its surfaces. In this work, the effect of oxygen surface terminals has been reduced by replacing it with other surface terminals or thin layers of heteroatom at the interlayers. These resulted in increasing the interlayer spacing from 9.3 Å up to 12.5 Å with better flexibility properties, thereby facilitating electron/mass transports by exposing enough active surface areas. The carbon nanoplated MXene showed enhanced specific capacitance of 110 F/g at 2 mV/s in LiOH electrolytes for superior supercapacitor applications.

GRAPHICAL ABSTRACT




ARTICLE HISTORY

Received 31 December 2022
Accepted 2 September 2023

KEYWORDS

MXene; surface terminations; supercapacitor; intercalated ions; 2D materials; nanoplating; nanohybrids

CONTACT Noora Al-Qahtani  noora.alqahtani@qu.edu.qa  Center for Advanced Materials (CAM), Qatar University, Doha, Qatar; Prasun Banerjee  pbanerje@gitam.edu  Gandhi Institute of Technology and Management (GITAM) University, Multiferroic and Magnetic Material Research Laboratory, Bengaluru, Karnataka, India; Rajender Boddula  research.raaj@gmail.com  Center for Advanced Materials (CAM), Qatar University, Doha, Qatar.

© 2023 The Author(s). Published by Informa UK Limited, trading as Taylor & Francis Group

This is an Open Access article distributed under the terms of the Creative Commons Attribution-NonCommercial License (<http://creativecommons.org/licenses/by-nc/4.0/>), which permits unrestricted non-commercial use, distribution, and reproduction in any medium, provided the original work is properly cited. The terms on which this article has been published allow the posting of the Accepted Manuscript in a repository by the author(s) or with their consent.

1. Introduction

Hydrogen production from splitting water and electrochemical storage (ECs) energies are the benchmark way of energy conversion and clean energy storage [1,2]. Although the availability of different technologies mainly depends on the use of active material [3]. This material accelerates the electrochemical reactions with its superior reaction kinetics, smooth charge transfer mechanism, robust structures, and available surface areas [4]. The adjustable surface functionalities and robust chemical, electrical, and physical properties of MXene-based materials make them natural choices for active materials [5]. MXenes are the layered structure of stacked 2D sheets, such as $Ti_3C_2T_x$, where T_x are generally fluorine, oxygen, and hydroxyl surface termination groups shown in Figure 1 [6]. This helps to build tunable properties with a hydrophilic surface in MXene material with metallic properties [7], whereas chemically functionalized graphene shows the electrical conductivity degradation. Both the materials' Van der Waals interaction interconnect the adjacent layers [8]. Most of the synthesis methods use fluoride-based materials [9–11]. This results in absolutely no control over the positions of the terminals across the 2D sheets [12]. They can be randomly distributed with (I) the transitional metal ions or will stack with (II) the X atoms or with a combination of (I) and (II) together [13].

The thermodynamical calculations and Bader charge analysis clearly indicate the preference of oxygen functional groups as it requires two electrons, which can easily stabilize the two interconnected layers with interstitial bonding [14]. This property makes the MXene material metastable at room temperature [15]. At a higher temperature, MXene transformed into a more stable oxide compound from the carbide or nitride stage [16]. Hence, the surface oxidation of MXene results in its poor performance as an active material [17]. This

phenomenon is nearly unavoidable in most of the general approaches such as calcination [18], refluxing [19], and solvothermal or hydrothermal synthesis [20]. This ultimately affects the fabrication of the MXene-based 2D materials as active materials for the ECs [21].

This work presents an efficient way to reduce the oxygen functional group for better electrochemical behavior [22]. We proposed that the effect of the oxygen functional group can be reduced in two ways: either by replacing it as much as possible with the other two functional groups [23], i.e. hydroxyl and fluorine group, or with the use of a very thin physical barrier that shields the effect of oxygen diffusion [24].

The use of hydrofluoric acid during synthesis inevitably introduces more $-F$ functional groups in MXene structure [25] while the use of $LiOH$ at ambient conditions increases the $-OH$ surface groups in the interlayers [26]. Wen et al. represented 192 F/g of capacitance when the heteroatom nitrogen is introduced between the interlayers with the use of ammonia [27]. Zhu et al. used the carbon nanoplating technique with good material compatibility [28], stability [29], and conductivity of the MXene-based materials [30].

Inspired by this work, we represent a comparative study between HF -treated MXene, alkaline MXene treated with $LiOH$, heteroatom-implanted MXene with ammonia, and carbon nanoplated MXene by the carbonization of glucose. These four nanohybrids are fabricated to demonstrate their applications for energy storage and conversion applications with superior stability [31].

2. Synthesis

2.1. MXene

To prepare the layered MXene sheets, 2 g of MAX phase powder (99.1%, Nanochemazone) was

"Surface Termination Group of MXene"

1	2	3	4	5	6	7	8	9	10	11	12	13	14	15	16	17	18	19	20	
1	H Hydrogen 1.008	He Helium 4.003																		
2	Li Lithium 6.941	Be Beryllium 9.012	B Boron 10.811	C Carbon 12.011	N Nitrogen 14.007	O Oxygen 15.999	F Fluorine 18.998	Ne Neon 20.180												
3	Na Sodium 22.990	Mg Magnesium 24.305	Al Aluminum 26.982	Si Silicon 28.086	P Phosphorus 30.974	S Sulfur 32.065	Cl Chlorine 35.453	Ar Argon 39.948												
4	K Potassium 39.098	Ca Calcium 40.078	Sc Scandium 44.956	Ti Titanium 47.88	V Vanadium 50.942	Cr Chromium 51.996	Mn Manganese 54.938	Fe Iron 55.845	Co Cobalt 58.933	Ni Nickel 58.693	Cu Copper 63.546	Zn Zinc 65.38	Ga Gallium 69.723	Ge Germanium 72.630	As Arsenic 74.922	Se Selenium 78.96	Br Bromine 79.904	Kr Krypton 83.798		
5	Rb Rubidium 85.468	Sr Strontium 87.62	Y Yttrium 88.906	Zr Zirconium 91.224	Nb Niobium 92.906	Mo Molybdenum 95.94	Tc Technetium 98.906	Ru Ruthenium 101.07	Rh Rhodium 102.905	Pd Palladium 106.42	Ag Silver 107.868	Cd Cadmium 112.414	In Indium 114.818	Sn Tin 118.710	Sb Antimony 121.757	Te Tellurium 127.6	I Iodine 126.905	Xe Xenon 131.29		
6	Cs Cesium 132.905	Ba Barium 137.327	Lanthanoids	Hf Hafnium 178.49	Ta Tantalum 180.948	W Tungsten 183.84	Re Rhenium 186.207	Os Osmium 190.23	Ir Iridium 192.222	Pt Platinum 195.084	Au Gold 196.967	Hg Mercury 200.59	Tl Thallium 204.383	Pb Lead 207.2	Bi Bismuth 208.980	Po Polonium 209	At Astatine 210	Rn Radon 222		
7	Fr Francium 223	Ra Radium 226	Actinoids	Rf Rutherfordium 261	Db Dubnium 262	Sg Seaborgium 263	Bh Bohrium 264	Hs Hassium 265	Mt Meitnerium 266	Ds Darmstadtium 267	Rg Roentgenium 268	Cn Copernicium 269	Nh Nihonium 270	Fl Flerovium 277	Mc Moscovium 278	Lv Livermorium 279	Ts Tennessine 281	Og Oganesson 284		

M TRANSITION METAL
X C, N
T SURFACE TERMINATION

Figure 1. Schematic showing the surface termination groups of MXene.

dissolved in 100 mL HF (40% conc.) and consistently heated at a temperature 35 °C for 72 h to get rid of aluminium layers [32]. This acid was then neutralized until the pH value reached 4.1 with water and ethanol wash, and then vacuum desiccated at 60 °C. Finally, the black powder obtained was named as MXn [33].

2.2. Alkaline Mxene

To prepare alkaline Mxene, according to the molecular weight of LiOH, 4.196 g of it was dissolved in 100 mL of deionized water until a clear solution was achieved [34]. Added 4 g of Mxene powder to it and stored for 24 h at room temperature. Later, a water wash and an ethanol wash were performed until the pH value reached 9.3 and allowed to dry. Later, it was vacuum desiccated at 60 °C, and finally, the powder was designated as Alk-MXn [35].

2.3. Mxene@C

To prepare carbon-infused Mxene nanosheets, 0.4 g of Mxene was taken in 100 mL DDI water and kept for ultrasonication for about 1 h [36]. In another beaker, 4 g of dextrose (anhydrous) was dissolved in 50 mL DDI water and ultrasonicated for 60 min. Both solutions were transferred to the Teflon liner and kept in a furnace under 160 °C for 24 h. Later, it was subjected to a water and ethanol wash. Finally, the material was vacuum desiccated at 60 °C and named MXn@C [37].

2.4. Mxene@N

To prepare nitrogen-infused Mxene nanosheets, 0.4 g of Mxene was dissolved in 150 mL ammonia and ultrasonicated for 1 h [38]. Then, it was kept in the furnace at 200 °C for 8 h. Later, it was given a water and ethanol wash. Finally, the material was vacuum desiccated at 60 °C and named MXn@N [39].

3. Sample characterization

Bruker D2 phaser X-ray diffractometer with Cu K radiation as a source ($\lambda = 0.1542$ nm) and high-resolution Lynxeye detector were used to analyse the X-ray diffraction data of the samples. Diffraction patterns of the samples were catalogued in the 2θ range of ($5^\circ \leq 2\theta \leq 80^\circ$) with a step scan range of $0.02^\circ \text{ s}^{-1}$ at room temperature. FTIR (PerkinElmer system 2000) was used to perform a spectroscopic investigation to analyse surface functional groups in the wavelength range of $500\text{--}4000 \text{ cm}^{-1}$. A programmed

LCR-bridge (Hioki HM8118) was used to estimate the dielectric measurement to explore the impedance characteristics over the frequency range of 20 Hz to 200 KHz. Electrochemical studies were performed using a Biologic Potentiostat–Galvanostat instrument. Cyclic voltammetry studies were done using a 25 mL glass cell with LiOH aqueous solution as an electrolyte, a Pt rod as a counter electrode, and a saturated calomel electrode (SCE) used as a reference electrode. Stainless steel mesh, due to its characteristic of high potential towards O_2 evolution, was used as a current collector. The electrode was prepared by coating stainless steel mesh with a slurry of active material (80%), acetylene black (10%), polytetrafluoroethylene (PTFE) binder (10%), and finally a few drops of solvent (N-methyl-2-pyrrolidone). The fabricated electrode was studied, and parameters were recorded. Equation of states calculation was carried out using the software Burai.

4. Results and discussion

4.1. Morphological-dependent performance of different MXenes

4.1.1. Mono-M MXenes

Ti_2CT_x , a member of 2D materials, is the mono M-MXene produced by etching the MAX phase Ti_2AlC . The aluminium stacks are taken out of the MAX phase by etching them with HF. Ti_2CT_x forms the subsequent lamellar sheets with a surface decorated with functional groups like $-OH$, $-F$, and $-O$. The functional groups make the MXene hydrophilic and dispersive, whereas density functional theory (DFT) reveals the carbon vacancies are Ti_2CT_x more flexible and conductive. The thermal stability of the material was found to be optimum in a vacuum or inert gas atmosphere only.

$Ti_3C_2T_x$, MXene is a mono M-MXene produced by etching the Ti_3AlC_2 MAX phase. The aluminium layer is etched from MAX powder by treating it with HF or $LiF + HCl$. Various characterization reveals the marked difference between bulk Ti_3AlC_2 and $Ti_3C_2T_x$ nanosheets. Scanning electron microscopy shows that the Ti_3AlC_2 are bulk and densely layered materials, while the obtained $Ti_3C_2T_x$ are accordion-like regular 2D sheets. XRD data shows the elimination of the Al layer as the peak at 39° disappears in MXene. Even the peak at 9.7° gets shifted to lower values, indicating spacing between the layers. Atomic force and transmission electron microscopy show very thin, flexible, and transparent nanosheets produced. Fabricated $Ti_3C_2T_x$ was treated at medium temperature to get annealed MXene. The loss of T_x hanging on the surface was caused by this thermal decrease. Annealed $Ti_3C_2T_x$, when combined with epoxy, showed better

characteristics at a loading of 15 wt% for electrochemical properties.

In the MXene family, another mono M-MXene is niobium carbide (Nb_2CT_x). As reported, Nb_2CT_x niobium carbide, when compared to Ti_2CT_x , is quite thinner because of increased inter-layer spacing and surface-enriched functional groups. The space between layers increases as two Nb layers get twisted over the carbon layer, but the bond angle and bond length are identical to Ti_2CT_x . Nb_2CT_x niobium carbide MXene is synthesized by eliminating the aluminium from Nb_2AlC . Studied by a group of researchers, variation of etching time, and chemical exfoliation varies the stacking order of the MXene layers, causing delamination of a few layers at 72 h. Revealed by scanning electron microscopy, the bulk phase of Nb_2AlC changes to lamellar sheets after etching with HF, verifying the removal of the aluminium layer. XRD data showed the extent of Al layer removal in different etching time conditions. Likewise, TEM, Raman, HRTEM, and TGA analysis verified the preparation of the niobium carbide. The EMI absorbing capacity of chemically exfoliated lamellar Nb_2CT_x niobium carbide was investigated when it was combined with paraffin wax nanocomposite. Nb_2CT_x niobium carbide (M2X) exhibits fewer atomic layers as compared to M3X and M4X, as a result of which it shows high gravimetric capacitance. It also is magnetic and superconductive in nature.

4.1.2. Double-X MXene

Ti_3CNT_x is a type of MXene with two X in the series, i.e. carbon and nitrogen forming double-X MXene. Ti_3CNT_x was synthesized by etching Ti_3AlCN powders with HF to get rid of the Al layer from the composite. When washed with deionized water and the collected sample was sonicated under an argon atmosphere, the final products obtained were dark green in colour. While 2D materials are well-known EMI shielding materials, double X-Mxene composites are investigated to check their EM wave-absorbing capacity. It was reported that when Ni@C microcubes were incorporated with 2D Ti_3CNT_x MXene, a layered porous composite was obtained. Various characterizations revealed the composite to be highly magnetic, electrically conductive, and properly stacked with numerous porous interfaces. Thus, EMI shielding measurements showed an efficiency of 66.7 dB for 60 mm thickness. The EMI absorbing mechanism includes electronic transport on the surface, followed by dipolar polarization accompanied by magnetic coupling and then repeated internal reflections within lamellar porous layers. $Ti_3CNT_x/Ni@C$ showed good joule energy

conversion, making the MXene a good candidate for EM wave shielding and energy conversion.

4.1.3. Double-M MXenes

Molybdenum-based MXene, like 2D $Mo_2TiC_2T_x$, is double-M MXene and belongs to the MXene family with two transition metals. In this type of double-M carbides, the Mo atoms form the outermost layer, which encapsulates Ti layers. These Mo-based two-metal MXenes are prepared using ternary and quaternary carbide powders like $Mo_2TiC_2T_x$, Mo_2Ga_2C , and $Mo_2Ti_2AlC_3$ as starting materials. These MAX phase powders are etched using HF, because of which the metallic bond between the transition metals and aluminium breaks, and aluminium gets removed. After proper washing, the final material is obtained. Various characterization like XRD, SEM, and Raman show the proper formations of the desired material. As reported, the $Mo_2TiC_2T_x$ shows a conductivity of nearly 120 S/cm. From the plot of temperature versus conductivity, it was found that the orderly stacked, $Mo_2TiC_2T_x$ exhibits metallic behaviour. Mo-based MXenes are reported to be thermally stable, highly conductive, and have a large thermoelectric power factor. Showing the efficiency of good EMI shielding and electrochemical properties of Mxene composite. Hence, overall, the high capacitance behaviour of MXene is mostly influenced by the M element, flake size, surface chemistry, surface groups, etc.

4.2. X-Ray diffraction

Figure 2 depicts the XRD pattern for the MAX phase and all MXene samples. The selective etching of the Al layers from the MAX phase powder with HF treatment leads to the absence of (104) aluminium peak at the 2θ value of 38.9° [40]. However, the presence of other characteristic peaks at 7.76° , 16.96° , 26.14° , 32.98° , 35.54° , 37.48° , 40.48° , 59.40° , and 65.48° , with their miller indices of (002), (004), (006), (100), (102), (103), (105), (9110), and (1011) respectively clearly indicate retainment of its hexagonal phase with $P63/m$ group of symmetry [41]. In general, the complete termination of the $-F$ group in Mxene samples leads to no obvious change in the interlayer spacing. However, the presence of the $-F$ surface group in HF-treated Mxene shifts the characteristic (002) peak from 9.5° to 7.76° for it; this indicates a d-spacing of 11.40 Å for the HF-treated Mxene phase [42]. The nanoplating with carbon, $-OH$ implantation, and N heteroatom presence enhance the d-spacing further to 11.84 Å, 12.48 Å, and 12.5 Å, respectively, the characteristic peak of (002) plane of amorphous carbon obtained for MXn@C sample at the 2θ value of 20° as well. The

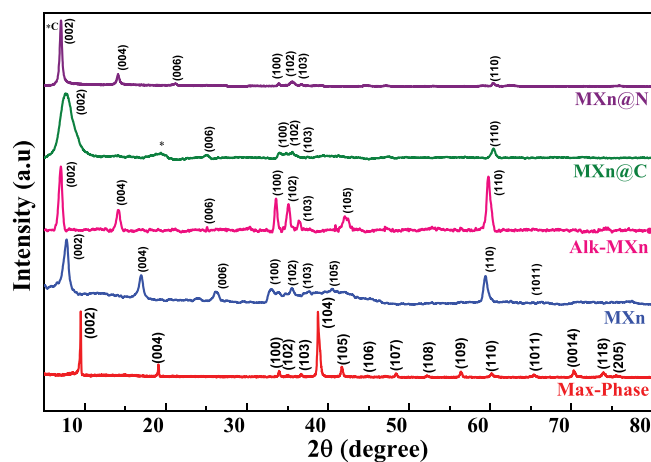


Figure 2. XRD Pattern of Max phase, MXn, Alk-MXn, MXn@C, and MXn@N.

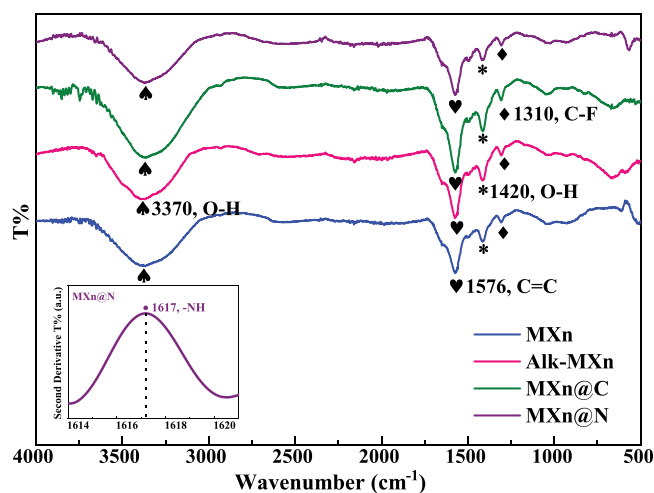


Figure 3. FTIR Spectrum of MXn, Alk-MXn, MXn@C, and MXn@N.

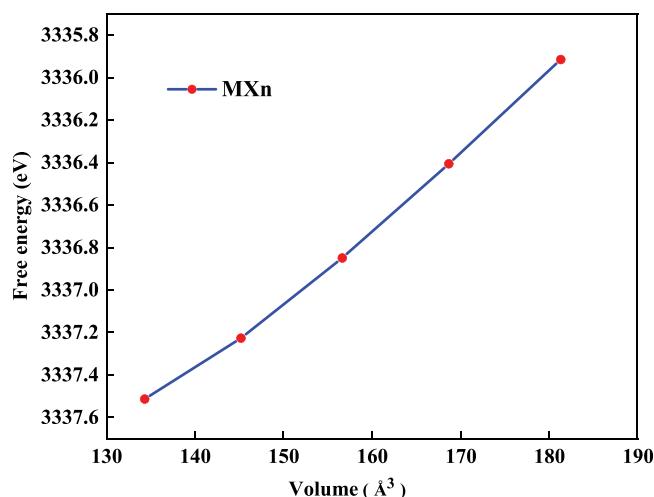


Figure 4. Free energy vs volume graph for MXene.

absence of a TiO_2 (101) peak in all the samples clearly indicates the disappearance of the effect of the oxidation in Mxene and any harmful carbonaceous material during the hydrothermal synthesis [43].

4.3. Fourier-transform infrared spectroscopy

The presence of surface functional groups has been verified with the FTIR spectroscopy shown in Figure 3. Interestingly, peaks corresponding to $-F$ and $-OH$ functional groups appear prominently in the

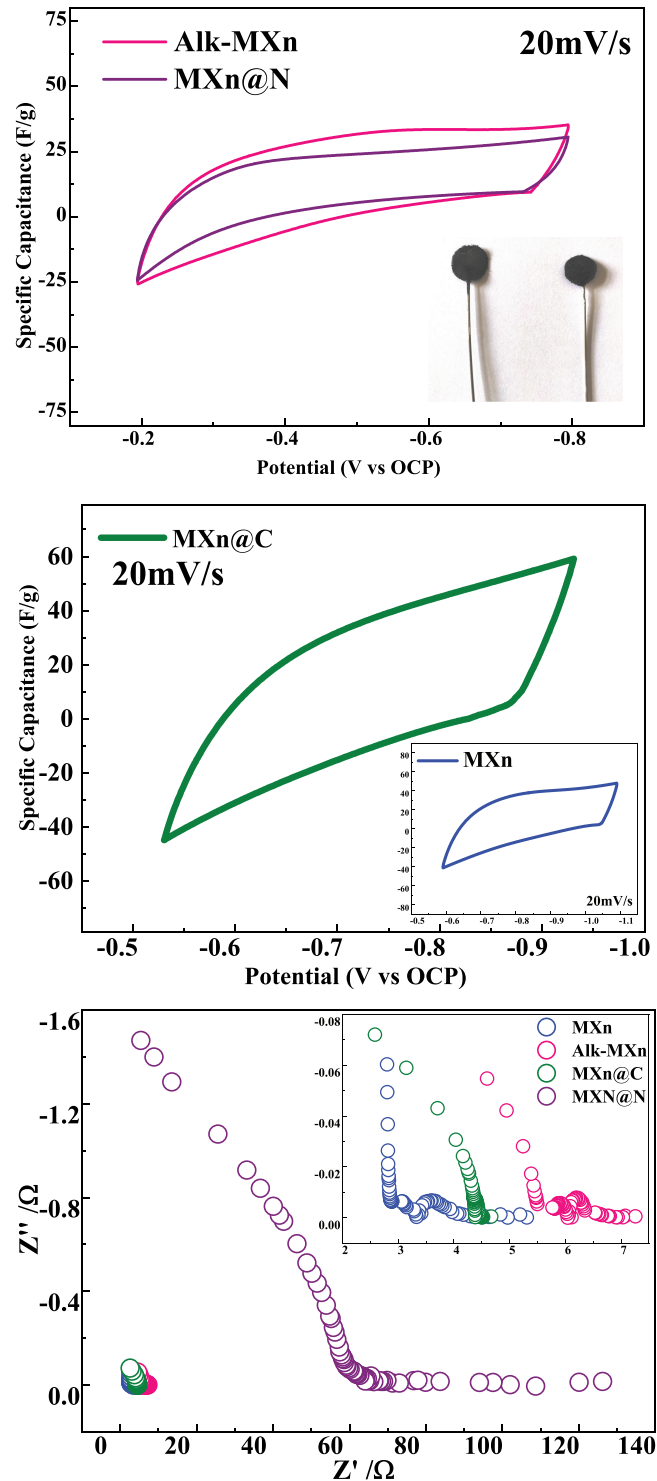


Figure 5. Electrochemical performance of MXn, Alk-MXn, MXn@C, and MXn@N electrodes.

spectrum. $C-F$ stretching vibrations are observed at 1310 cm^{-1} for all the Mxene samples. The band at 1420 cm^{-1} and 3370 cm^{-1} is identified as $-OH$ functional groups. These peak intensities were reduced for the MXn@N sample [44]. This may be due to the amalgamation of nitrogen at the Mxene matrices by reducing the surface functional groups of $-OH$. The hidden band of the $-NH$ group for MXn@N was deconvoluted using derivative spectroscopy shown in the inset of Figure 3. The presence of five hydroxyl groups in dextrose may be responsible for higher intensities of the $-OH$ band for the MXn@C sample.

The double-bonded carbon ($C=C$) band at 1576 cm^{-1} is the most intense for MXn@C sample because of the carbon nanoplating within the 2D layers. The absence of $C=O$ and $Ti-O$ stretching vibrations from the FTIR spectra indicates suppression of $-O$ functional groups in the 2D materials [45].

4.4. Simulated equations of state calculation

Structural optimization calculation was performed using DFT simulation techniques to understand the structural and atomic spacing behavior of Mxene. We

Table 1. Comparison table of electrochemical performances of MXene at 2 mV/s scan rates.

Sl No	Electrolyte	Specific capacitance (F/g)	Reference
1	MgSO ₄	97	[55]
2	K ₂ SO ₄	81	[55]
3	Mg(NO ₃) ₂	77	[55]
4	KOH	72	[55]
5	LiOH	110	Present work

Table 2. Specific capacitance of the material at different scan rates.

Scan rate (mV/s)	MXn	Specific Alk-MXn	Capacitance MXn@C	(F/g) MXn@N
2	40	42	110	42
5	39	34	97	32
10	35	30	88	27
20	31	26	59	22
50	24	19	38	15
100	17	14	29	11

formulated Mxene layers associated with their functional groups with the presence of a vacuum within the interlayers space along the Z-axis. The thermodynamic property was calculated with a given volume using $F = E_{DFT} + F_{VIB}$. Here, F represents the Helmholtz free energy, F_{VIB} is the vibrational free energy, and E_{DFT} is the DFT total energy [46]. We determined the Helmholtz free energies of the Mxene by the application of 25% deformation of their original volume. Finally, the equation of states was obtained by fitting such fire different volumes under biaxial deformation tensors, as shown in Figure 4. The absence of minima in the free energy calculations indicates towards non-equilibrium states [47]. Hence, the presence of other functional groups makes the Mxene flexible, but the strength might be higher with the $-O$ functional group. The mechanical exfoliation of the graphene sheet shows a linear graph because of the presence of strong van der Waals interactions between the 2D layers. Hence, the presence of the other functional groups has a stronger effect on the bond strength of the Mxene [48].

4.5. Electrochemical performances

Electrochemical analysis has been performed to understand the effect of the surface functional group on the super capacitive behavior of the Mxene. Open circuit potential (OCP) has been taken as the starting potential to avoid oxidation in LiOH electrolytes [49]. With a scan rate of 20 mV/s, the cyclic voltograms of Alk-MXn and MXn@N are displayed in Figure 5(a). Both materials show almost similar and quasi-rectangular shapes [50]. This similar nature may be due to the similar interlayer spacing between the materials as obtained during XRD analysis. The electrochemical performances of MXn and MXn@C enhance with the higher integrated area than their counterparts at room temperature shown in Figure 5(b). The more idealistic

rectangular shape was observed during the charge cycle because of faster intercalation of the Li^+ cations. This might be due to the enhanced conductivity with the presence of $-F$ and nanoplated carbon in MXn and MXn@C, respectively. MXn@C samples were found to have the highest specific capacitance, measuring 110 F/g at a 2 mV/s scan rate. The electrochemical performance of the Mxene in comparison to the LiOH as an electrolyte has been presented in Table 1.

The impedance behavior of the material presented with the Nyquist plot is shown in Figure 5(c). It depicts the information about the conductivity mechanism of the sample. Here, MXn and Alk-MXn show two semicircles and a slope line, whereas MXn@C exhibited a single semicircle with a slope, and MXn@N showed only a slope line with no greater semicircle. This clearly helps us understand the charge transfer resistance of the samples [51]. The MXn material shows a low impedance value with low charge transfer resistivity exhibiting higher conductivity with the presence of $-F$ ions [52]. Similarly, Alk-MXn and MXn@C also resemble the near similar properties to MXn [53]. But MXn@N shows different conductivity compared to all other samples. The Nyquist plot's shape gives information on the physical processes taking place at conductive junctions [54].

5. Conclusions

In summary, we developed an efficient way to reduce the oxygen functional groups in 2D MXene. Compared with the pristine MXene, the presence of the $-OH$ and $-F$ surface terminal groups or the presence of a very thin layer of carbon or nitrogen atoms show better electrochemical behavior in the 2D material. The simulation studies represent that the reduction of the oxygen functional groups leads towards non-equilibrium free energies, which makes the material more flexible. The XRD and FTIR analysis shows that the modification process of surface terminals or the high-temperature nanoplating retains the original accordion structure of the 2D material, thereby facilitating electron transports by exposing more than enough active surface areas for super capacitor applications. A superior 110 F/g specific capacitance can be achieved with MXn@C samples at 2 mV/s scan rate shown in Table 2. This provides much more insight into the high-performance super capacitors with the design and modulations of the surface terminals in MXene-based 2D materials.

Acknowledgements

Open Access funding was provided by the Qatar National Library. P. Banerjee received financial assistance from SERB, India with grant no TAR/2021/000032. B. Koneru thank SJS GC [F. No. 82-7/2022(SA-III)] UGC JRF

research fellowship and J. Swapnalini acknowledge GITAM University for a T. A. fellowship. P. Banerjee acknowledges that the work reported here was supported in part by I-STEM program, funded by the Office of the Principal Scientific Adviser to the Govt. of India.

Author statements

Conceptualization: Rajender Boddula, Noora Al-Qahtani, and Prasun Banerjee; Methodology: Bhargavi Koneru and Ahmed Bahgat Radwan; Validation: Rajender Boddula and Prasun Banerjee; Resources: Ahmed Bahgat Radwan and Ramyakrishna Pothu; Data curation: Bhargavi Koneru, Ramyakrishna Pothu, and Jhilmil Swapnalini; Writing: original draft preparation, Prasun Banerjee; Writing: review and editing, Rajender Boddula and Noora Al-Qahtani; Visualization: Bhargavi Koneru, Ahmed Bahgat Radwan, and Jhilmil Swapnalini; Supervision: Noora Al-Qahtani and Rajender Boddula; Project administration: Rajender Boddula and Prasun Banerjee; Funding acquisition: Noora Al-Qahtani and Prasun Banerjee. All authors have read and agreed to the published version of the manuscript.

Disclosure statement

No potential conflict of interest was reported by the author(s).

Funding

This work was supported by Qatar University through a National Capacity Building Program Grant (NCBP) [QUCP-CAM-2022-463]. The publication of the article was funded by the Qatar National Library. Statements made herein are solely the responsibility of the authors.

Notes on contributors

Bhargavi Koneru is a doctoral researcher at the Gandhi Institute of Technology and Management (GITAM) University, India. She is working on the research domain of synthesis and characterization of MXene/Bismuth Ferrite 2D hierarchical structure.

Jhilmil Swapnalini is a doctoral researcher at the Gandhi Institute of Technology and Management (GITAM) University, India. She is underlining the research studies of some physical properties of CoFe_2O_4 intercalated $\text{Ti}_3\text{C}_2\text{T}_x$ -based two-dimensional layered composites.

Ramyakrishna Pothu is currently pursuing her PhD degree in chemistry under the supervision of Prof. Jianmin Ma in the Hunan University (China). She obtained her Bachelor degree from Satavahana University, India in 2013, and her Postgraduate degree from Osmania University, India in 2015, respectively. She has published several scientific articles in peer-reviewed international journals and co-authored more than twenty book chapters by various publishers. Her main research interests focus on the functional nanomaterials and its composites for energy and environmental science.

Dr. Prasun Banerjee holds a B.Sc. (Hons.) degree in Physics (2002), a Master's in Physics (2004) and a PhD in Physics (2011) from University of Calcutta, India, post-doctorate in Physics (2014-2017) from the Universidade

Federal de Goiás, Goiânia. He is an Associate Professor at the Gandhi Institute of Technology and Management (GITAM) University, India. He has experience in Condensed Matter Physics, emphasizing the preparation and characterization of MXene 2D materials for the multifunctional energy harvester device to generate clean nano/micro energy.

Dr. Rajender Boddula received his Ph.D degree in Chemistry (2014) from Kakatiya University/CSIR-IICT, India, under the supervision of Dr. S. Palaniappan, Polymers & Functional Materials division. His academic honors include many merit scholarships and study-abroad fellowships from Australian Endeavour Research fellowship and Chinese Academy of Sciences-President's International Fellowship Initiative (2016). He has authored around eighty international scientific papers, thirty book chapters, and serving as editorial board member and referee for reputed international peer-reviewed journals. He has published edited books with Springer, Elsevier, and Wiley. His specialized areas of sustainable energy & fuels, which include nanomaterials, graphene, polymer composites.

Ahmed Bahgat Radwan obtained his Ph.D. degree in inorganic chemistry from Ain Shams University. Since 2014, he has been working as a senior researcher in the Centre for Advanced Materials at Qatar University. His research interests focus on material science and physical chemistry. He has expertise in multidisciplinary research areas including failure analysis of metals, self-healing epoxy coatings, electrodeposition, biodegradable alloys, and preparation of nanomaterials and mesoporous materials. Ahmed Bahgat Radwan has had the privilege of securing several grants to support various research initiatives and projects with a total fund of 740,000 \$ at Qatar University as a principal investigator.



Dr. Noora Al-Qahtani as Acting Head of Central Lab Unit and Research Assistant Professor at the Center for Advanced Materials (CAM), Qatar University (QU), was awarded her BSc in Physics and Biomedical Sciences from the College of Arts and Sciences at Qatar University in 2008. Then, she pursued her MSc and PhD degrees at the University of Sheffield, UK, and Imperial College London, UK, in 2015 and 2020, respectively. Dr. Noora is the first Qatari female whose PhD is in corrosion.

During her academic career, Dr. Al-Qahtani has chaired and participated in many projects and committees at QU. In addition, Dr. Noora's collaboration within QU and international research groups is remarkable. Moreover, she is a member of many professional organizations and participated in various training sessions and workshops focusing on strategic management, research administration, international relations, and education strategies. Dr. Al-Qahtani is also one of the founders and was, for a long period, a leading member of the Al-Bairaq team, which has received numerous local and international awards.


Dr. Noora Al-Qahtani's experience exceeds 15 years in both academia and industry. Her impressive record, with over 50 articles, has been published in well-reputed, high-impact peer-reviewed journals and conference proceedings. Dr. Al-Qahtani has been awarded, independently and in collaboration with other researchers, many grants from Qatar University. For instance, she is a key

investigator in three mega projects funded by the Qatar National Research Fund (NPRP), worth more than 1.9 million USD. Dr. Al-Qahtani received multiple awards from renowned organizations worldwide. In 2023, she was honored with the Best Researcher Award at the 5th Edition of the International Research Awards on Advanced Nanomaterials and Nanotechnology.

ORCID

Bhargavi Koneru  <http://orcid.org/0009-0005-5835-2222>
 Jhilmil Swapnalini  <http://orcid.org/0000-0001-9052-3398>

Ramyakrishna Pothu  <http://orcid.org/0000-0002-5806-9583>

Prasun Banerjee  <http://orcid.org/0000-0001-8473-6610>
 Rajender Boddula  <http://orcid.org/0000-0001-8533-3338>

Ahmed Bahgat Radwan  <http://orcid.org/0000-0003-1115-3590>

Noora Al-Qahtani  <http://orcid.org/0000-0001-8535-2731>

References

- Zhang Y, Liu J, Li S-L, et al. Polyoxometalate-based materials for sustainable and clean energy conversion and storage. *Energy Chem.* 2019;1:100021. doi: [10.1016/j.enchem.2019.100021](https://doi.org/10.1016/j.enchem.2019.100021).
- Ghosh T, Koneru B, Banerjee P. Artificial intelligence for energy conversion. *Appl Artificial Intell New Mater Discovery.* 2023;147:123–138.
- Koneru B, Swapnalini J, Natarajan S, et al. Investigation of the ion dynamics by a particular excitation due to the stoichiometric imbalances on BiFeO₃ ceramics. *Physica B.* 2023;649:414463. doi: [10.1016/j.physb.2022.414463](https://doi.org/10.1016/j.physb.2022.414463).
- Zhang B-W, Wang Y-X, Chou S-L, et al. Fabrication of superior single-atom catalysts toward diverse electrochemical reactions. *Small Methods.* 2019;3:1800497. doi: [10.1002/smt.201800497](https://doi.org/10.1002/smt.201800497).
- Koneru B, Swapnalini J, Natarajan S, et al. Intercalation of nanoscale multiferroic spacers between the two-dimensional interlayers of MXene. *ACS Omega.* 2022;7:20369–20375. doi: [10.1021/acsomega.2c02471](https://doi.org/10.1021/acsomega.2c02471).
- Swapnalini J, Koneru B, Pothu R, et al. Surface modification of Ti₃C₂T_x using terminal groups and heteroatoms with excellent electrochemical performance in supercapacitors. *Appl Phys Lett.* 2023;122:161902. doi: [10.1063/5.0142053](https://doi.org/10.1063/5.0142053).
- Kumar JA, Prakash P, Krithiga T, et al. Methods of synthesis, characteristics, and environmental applications of MXene: a comprehensive review. *Chemosphere.* 2022;286:131607. doi: [10.1016/j.chemosphere.2021.131607](https://doi.org/10.1016/j.chemosphere.2021.131607).
- Burdanova MG, Liu M, Staniforth M, et al. Intertube excitonic coupling in nanotube Van der Waals heterostructures. *Adv Funct Mater.* 2022;32:2104969. doi: [10.1002/adfm.202104969](https://doi.org/10.1002/adfm.202104969).
- Hu M, Zhang H, Hu T, et al. Emerging 2D MXenes for supercapacitors: status, challenges and prospects. *Chem Soc Rev.* 2020;49:6666–6693. doi: [10.1039/d0cs00175a](https://doi.org/10.1039/d0cs00175a).
- Chao H, Qin H, Zhang M, et al. Boosting the pseudocapacitive and high mass-loaded lithium/sodium storage through bonding polyoxometalate nanoparticles on MXene nanosheets. *Adv Funct Mater.* 2021;31:2007636. doi: [10.1002/adfm.202007636](https://doi.org/10.1002/adfm.202007636).
- Wang C, Yang H, Wang B, et al. Dual cation doping enabling simultaneously boosted capacity and rate capability of MnO₂ cathodes for Zn//MnO₂ batteries. *Nano Res.* 2023;16:9488–9495. doi: [10.1007/s12274-023-5717-8](https://doi.org/10.1007/s12274-023-5717-8).
- Tang R, Xiong S, Gong D, et al. Ti₃C₂ 2d MXene: recent progress and perspectives in photocatalysis. *ACS Appl Mater Interfaces.* 2020;12:56663–56680. doi: [10.1021/acsami.0c12905](https://doi.org/10.1021/acsami.0c12905).
- Zuo G, Wang Y, Teo WL, et al. Ultrathin ZnIn₂S₄ nanosheets anchored on Ti₃C₂T_x MXene for photocatalytic H₂ evolution. *Angewandte Chemie.* 2020;132:11383–11388. doi: [10.1002/ange.202002136](https://doi.org/10.1002/ange.202002136).
- Zhang H, Fang Y, Yang F, et al. Aromatic organic molecular crystal with enhanced π–π stacking interaction for ultrafast Zn-ion storage. *Energy Environ Sci.* 2020;13:2515–2523. doi: [10.1039/D0EE01723J](https://doi.org/10.1039/D0EE01723J).
- Swapnalini J, Koneru B, Boddula R, et al. 2D nanomaterials as lubricant additives. In: Nadda AK, Nguyen TA, Sharma S, Bilal M, Gupta RK, editors. *Nanotechnology for Advanced Biofuels.* Elsevier; 2023. p. 97–112.
- Wyatt BC, Nemani SK, Desai K, et al. High-temperature stability and phase transformations of titanium carbide (Ti₃C₂T_x) MXene. *J. Phys.* 2021;33:224002. doi: [10.1088/1361-648X/abe793](https://doi.org/10.1088/1361-648X/abe793).
- Liu Y, Jiang Y, Hu Z, et al. In-situ electrochemically activated surface vanadium valence in V₂C MXene to achieve high capacity and superior rate performance for Zn-ion batteries. *Adv Funct Mater.* 2021;31:2008033. doi: [10.1002/adfm.202008033](https://doi.org/10.1002/adfm.202008033).
- Pu L, Zhang J, Kuate Loic Jiresse N, et al. N-doped mxene derived from chitosan for the highly effective electrochemical properties as supercapacitor. *Adv Compos Hybrid Mater.* 2022;5:356–369. doi: [10.1007/s42114-021-00371-5](https://doi.org/10.1007/s42114-021-00371-5).
- Lu C, Li A, Zhai T, et al. Interface design based on Ti₃C₂ MXene atomic layers of advanced battery-type material for supercapacitors. *Energy Storage Mater.* 2020;26:472–482. doi: [10.1016/j.ensm.2019.11.021](https://doi.org/10.1016/j.ensm.2019.11.021).
- Zhong Q, Li Y, Zhang G. Two-dimensional MXene-based and MXene-derived photocatalysts: recent developments and perspectives. *Chem Eng J.* 2021;409:128099. doi: [10.1016/j.cej.2020.128099](https://doi.org/10.1016/j.cej.2020.128099).
- VahidMohammadi A, Moncada J, Chen H, et al. Thick and freestanding mxene/pani pseudocapacitive electrodes with ultrahigh specific capacitance. *J Mater Chem A.* 2018;6:22123–22133. doi: [10.1039/C8TA05807E](https://doi.org/10.1039/C8TA05807E).
- El-Hallag IS, El-Nahass MN, Youssry SM, et al. Facile in-situ simultaneous electrochemical reduction and deposition of reduced graphene oxide embedded palladium nanoparticles as high performance electrode materials for supercapacitor with excellent rate capability. *Electrochim Acta.* 2019;314:124–134. doi: [10.1016/j.electacta.2019.05.065](https://doi.org/10.1016/j.electacta.2019.05.065).
- Leng L, Xu S, Liu R, et al. Nitrogen containing functional groups of biochar: an overview. *Bioresour Technol.* 2020;298:122286. doi: [10.1016/j.biortech.2019.122286](https://doi.org/10.1016/j.biortech.2019.122286).
- Li Y, Cao C-F, Li S-N, et al. In situ reactive self-assembly of a graphene oxide nano-coating in polymer foam materials with synergistic fire shielding properties. *J Mater Chem A.* 2019;7:27032–27040. doi: [10.1039/C9TA09372A](https://doi.org/10.1039/C9TA09372A).

25. Li L, Zhang Y-N, Zhou Y, et al. Optical fiber optofluidic bio-chemical sensors: a review. *Laser Photon Rev.* 2021;15:2000526. doi: [10.1002/lpor.202000526](https://doi.org/10.1002/lpor.202000526).
26. Peng L, Zhu Y, Chen D, et al. Two-dimensional materials for beyond-lithium-ion batteries. *Adv Energy Mater.* 2016;6:1600025. doi: [10.1002/aenm.201600025](https://doi.org/10.1002/aenm.201600025).
27. Wen Y, Rufford TE, Chen X, et al. Nitrogen-doped $Ti_3C_2T_x$ mxene electrodes for high-performance supercapacitors. *Nano Energy.* 2017;38:368–376. doi: [10.1016/j.nanoen.2017.06.009](https://doi.org/10.1016/j.nanoen.2017.06.009).
28. Jiang Q, Lei Y, Liang H, et al. Review of MXene electrochemical microsupercapacitors. *Energy Storage Mater.* 2020;27:78–95. doi: [10.1016/j.ensm.2020.01.018](https://doi.org/10.1016/j.ensm.2020.01.018).
29. Li X, Huang Z, Zhi C. Environmental stability of MXenes as energy storage materials. *Front Mater.* 2019;6:312. doi: [10.3389/fmats.2019.00312](https://doi.org/10.3389/fmats.2019.00312).
30. Zhu Q, Li J, Simon P, et al. Two-dimensional mxenes for electrochemical capacitor applications: progress, challenges and perspectives. *Energy Storage Mater.* 2021;35:630–660. doi: [10.1016/j.ensm.2020.11.035](https://doi.org/10.1016/j.ensm.2020.11.035).
31. Meng W, Liu X, Song H, et al. Advances and challenges in 2d mxenes: from structures to energy storage and conversions. *Nano Today.* 2021;40:101273. doi: [10.1016/j.nantod.2021.101273](https://doi.org/10.1016/j.nantod.2021.101273).
32. Mathis TS, Maleski K, Goad A, et al. Modified max phase synthesis for environmentally stable and highly conductive Ti_3C_2 MXene. *ACS Nano.* 2021;15:6420–6429. doi: [10.1021/acsnano.0c08357](https://doi.org/10.1021/acsnano.0c08357).
33. Natu V, Pai R, Sokol M, et al. 2d $Ti_3C_2T_x$ MXene synthesized by water-free etching of Ti_3AlC_2 in polar organic solvents. *Chem.* 2020;6:616–630. doi: [10.1016/j.chempr.2020.01.019](https://doi.org/10.1016/j.chempr.2020.01.019).
34. Zhang H, Wang Z, Shen Y, et al. Ultrathin 2d $Ti_3C_2T_x$ MXene membrane for effective separation of oil-in-water emulsions in acidic, alkaline, and salty environment. *J Colloid Interface Sci.* 2020;561:861–869. doi: [10.1016/j.jcis.2019.11.069](https://doi.org/10.1016/j.jcis.2019.11.069).
35. Lv Z, Ma W, Wang M, et al. Co-constructing interfaces of multiheterostructure on MXene ($Ti_3C_2T_x$)-modified 3d self-supporting electrode for ultraefficient electrocatalytic her in alkaline media. *Adv Funct Mater.* 2021;31:2102576. doi: [10.1002/adfm.202102576](https://doi.org/10.1002/adfm.202102576).
36. Lv L-P, Guo C-F, Sun W, et al. Strong surface-bound sulfur in carbon nanotube bridged hierarchical Mo_2C -based MXene nanosheets for lithium-sulfur batteries. *Small.* 2019;15:e1804338. doi: [10.1002/sml.201804338](https://doi.org/10.1002/sml.201804338).
37. Hu Y, Pang S, Yang G, et al. MXene modified carbon fiber composites with improved mechanical properties based on electrophoretic deposition. *Mater Res Bull.* 2022;150:111761. doi: [10.1016/j.materresbull.2022.111761](https://doi.org/10.1016/j.materresbull.2022.111761).
38. Shi H, Zhang CJ, Lu P, et al. Conducting and lithophilic MXene/graphene framework for high-capacity, dendrite-free lithium-metal anodes. *ACS Nano.* 2019;13:14308–14318. doi: [10.1021/acsnano.9b07710](https://doi.org/10.1021/acsnano.9b07710).
39. Bao W, Liu L, Wang C, et al. Facile synthesis of crumpled nitrogen-doped MXene nanosheets as a new sulfur host for lithium-sulfur batteries. *Adv Energy Mater.* 2018;8:1702485. doi: [10.1002/aenm.201702485](https://doi.org/10.1002/aenm.201702485).
40. Shuck CE, Han M, Maleski K, et al. Effect of Ti_3AlC_2 max phase on structure and properties of resultant $Ti_3C_2T_x$ MXene. *ACS Appl Nano Mater.* 2019;2:3368–3376. doi: [10.1021/acsanm.9b00286](https://doi.org/10.1021/acsanm.9b00286).
41. Meshkian R, Tao Q, Dahlqvist M, et al. Theoretical stability and materials synthesis of a chemically ordered MAX phase, Mo_2ScAlC_2 , and its two-dimensional derivate Mo_2ScC_2 MXene. *Acta Mater.* 2017;125:476–480. doi: [10.1016/j.actamat.2016.12.008](https://doi.org/10.1016/j.actamat.2016.12.008).
42. Feng A, Yu Y, Wang Y, et al. Two-dimensional MXene Ti_3C_2 produced by exfoliation of ti_3alc_2 . *Mater Design.* 2017;114:161–166. doi: [10.1016/j.matdes.2016.10.053](https://doi.org/10.1016/j.matdes.2016.10.053).
43. Li Z, Wang L, Sun D, et al. Synthesis and thermal stability of two-dimensional carbide MXene Ti_3C_2 . *Mater Sci Eng B.* 2015;191:33–40. doi: [10.1016/j.mseb.2014.10.009](https://doi.org/10.1016/j.mseb.2014.10.009).
44. Zhi W, Xiang S, Bian R, et al. Study of MXene-filled polyurethane nanocomposites prepared via an emulsion method. *Compos Sci Technol.* 2018;168:404–411. doi: [10.1016/j.compscitech.2018.10.026](https://doi.org/10.1016/j.compscitech.2018.10.026).
45. Sun Y, Xu D, Li S, et al. Assembly of multidimensional MXene-carbon nanotube ultrathin membranes with an enhanced anti-swelling property for water purification. *J Membr Sci.* 2021;623:119075. doi: [10.1016/j.memsci.2021.119075](https://doi.org/10.1016/j.memsci.2021.119075).
46. Wei B, Fu Z, Legut D, et al. Rational design of highly stable and active MXene-based bifunctional ORR/OER double-atom catalysts. *Adv Mater.* 2021;33:2102595. doi: [10.1002/adma.202102595](https://doi.org/10.1002/adma.202102595).
47. Pathak M, Sekhar Rout C. Hierarchical $NiCo_2S_4$ nanostructures anchored on nanocarbons and $Ti_3C_2T_x$ mxene for high-performance flexible solid-state asymmetric supercapacitors. *Adv Compos Hybrid Mater.* 2022;5:1404–1422. doi: [10.1007/s42114-022-00466-7](https://doi.org/10.1007/s42114-022-00466-7).
48. Vadym NB, Mochalin VN, Gogotsi Y. Bending rigidity of two-dimensional titanium carbide (mxene) nanoribbons: a molecular dynamics study. *Comput Mater Sci.* 2018;143:418–424.
49. Hu M, Hu T, Li Z, et al. Surface functional groups and interlayer water determine the electrochemical capacitance of $Ti_3C_2T_x$ MXene. *ACS Nano.* 2018;12:3578–3586. doi: [10.1021/acsnano.8b00676](https://doi.org/10.1021/acsnano.8b00676).
50. Yu T, Li S, Zhang L, et al. In situ growth of ZIF-67-derived nickel-cobalt-manganese hydroxides on 2d V_2CT_x MXene for dual-functional orientation as high-performance asymmetric supercapacitor and electrochemical hydroquinone sensor. *J Colloid Interface Sci.* 2022;629:546–558. doi: [10.1016/j.jcis.2022.09.107](https://doi.org/10.1016/j.jcis.2022.09.107).
51. Aguedo J, Lorencova L, Barath M, et al. Electrochemical impedance spectroscopy on 2d nanomaterial MXene modified interfaces: application as a characterization and transducing tool. *Chemosensors.* 2020;8:127. doi: [10.3390/chemosensors8040127](https://doi.org/10.3390/chemosensors8040127).
52. Yoon S-B, Jegal J-P, Chul Roh K, et al. Electrochemical impedance spectroscopic investigation of sodium ion diffusion in MnO_2 using a constant phase element active in desired frequency ranges. *J Electrochem Soc.* 2014;161:H207–H213. doi: [10.1149/2.046404jes](https://doi.org/10.1149/2.046404jes).
53. Ji B, Fan S, Kou S, et al. Microwave absorption properties of multilayer impedance gradient absorber consisting of $Ti_3C_2T_x$ MXene/polymer films. *Carbon.* 2021;181:130–142. doi: [10.1016/j.carbon.2021.05.018](https://doi.org/10.1016/j.carbon.2021.05.018).
54. Shen C, Wang L, Zhou A, et al. Synthesis and electrochemical properties of two-dimensional RGO/ $Ti_3C_2T_x$ nanocomposites. *Nanomaterials.* 2018;8:80. doi: [10.3390/nano8020080](https://doi.org/10.3390/nano8020080).
55. Lukatskaya MR, Mashtalir O, Ren CE, et al. Cation intercalation and high volumetric capacitance of two-dimensional titanium carbide. *Science.* 2013;341:1502–1505. doi: [10.1126/science.1241488](https://doi.org/10.1126/science.1241488).